EAI Endorsed Transactions
on Energy Web
Research Article EAI.EU

Dynamic Error Compensation Method for Binocular Ranging of Transmission Lines Integrating IMU Data

Zhimeng Zhang[1,*], Jie Liu[1], Cuiying Sun[1], Xiaoyu Yi[1] and Yixin Wang[1]

[1]Electric Power Research Institute of State Grid Hebei Electric Power Co., Ltd., Shijiazhuang, 050021, China

Abstract

This paper proposes a dynamic error compensation method that integrates inertial measurement unit (IMU) data. The initial distance is obtained based on the binocular vision triangulation ranging principle. By analyzing the dynamic error sources such as camera movement, cable vibration and environmental interference, the IMU multi-sensor is integrated to collect the system's motion, attitude and environmental parameters in real time. The IMU data is integrated and processed to calculate the compensation amount of multi-source errors. With the help of the PID controller, the proportional-integral-derivative operation and linear combination of the total compensation amount are carried out to achieve effective compensation of dynamic errors. Experiments show that this method can significantly improve the ranging stability under different working conditions, and the coefficient of variation is always lower than 0.2.

Keywords: IMU Data, Transmission Lines, Binocular Ranging, Sources of Dynamic Error, Error Compensation, PID Controller.

Received on 01 September 2025, accepted on 21 December 2025, published on 04 May 2026

doi: 10.4108/ew.12830

1. Introduction

In complex power system networks, transmission lines are prone to the influence of natural environments such as wind loads and temperature fluctuations, causing dynamic changes in their shape and spatial position [1-3]. Accurately measuring the distance between lines is crucial for preventing safety accidents. However, due to environmental interference, dynamic changes in targets and the limitations of measurement equipment, the existing measurement methods have problems of insufficient accuracy and poor reliability, which affect safety assessment and increase the risk of accidents [4-6]. Therefore, error compensation for the distance measurement of transmission lines is an urgent need to improve measurement accuracy, enhance monitoring capabilities, and ensure the stable operation of the power system [7].

Based on the above background, many scholars have conducted research on measurement error compensation and achieved certain results. For example, Kim H et al. used an RGB camera to capture visual image information of transmission lines, employed laser radar to obtain three-dimensional spatial data of the lines and their surrounding environment, integrated the two types of data, and then used full-scale structural displacement measurement technology to measure the overall displacement of the transmission lines. To improve measurement accuracy, a camera self-motion compensation algorithm was employed to eliminate measurement errors, thereby constructing a high-precision three-dimensional model of the transmission line. Based on this model, the displacement measurement results were calibrated and optimized to achieve distance measurement compensation for transmission lines [8]. However, while the camera self-motion compensation algorithm can eliminate

*Corresponding author. Email: 15931090169@163.com

measurement errors caused by the camera's own motion, it fails to achieve ideal compensation effects under extreme motion conditions, such as severe shaking or rapid rotation. Kim D H et al. employed an adaptive linear neural encoder to monitor the motor's current, position, and other operational parameters in real time, comparing these parameters with predefined ideal parameters to precisely identify deviations between actual operation and the theoretical model, i.e., measurement errors. Subsequently, FOC vector control technology was used to finely adjust the amplitude and phase of the current, while the STC algorithm was employed to dynamically optimize control parameters based on error changes, thereby achieving effective compensation for measurement errors [9]. However, the FOC vector control technique in this method is highly sensitive to changes in motor parameters and struggles to accurately track current amplitude and phase under complex operating conditions (such as high-speed motor operation, sudden load changes, or significant fluctuations in environmental temperature), leading to poor error compensation performance. Noh Y H et al. used high-precision current probes to precisely measure the output current of a single parallel current sensor, compared the measured results with theoretical values to obtain measurement errors, and conducted an in-depth analysis of the error sources from environmental factors (such as temperature, humidity, and electromagnetic interference) and circuit layout (such as wiring length, grounding method, and signal coupling). Based on the error analysis results, they employed techniques such as filtering and optimizing the circuit layout to compensate for the measurement errors, thereby improving the measurement accuracy [10]. Although filtering techniques can effectively suppress high-frequency noise, they also introduce new issues such as phase delay and amplitude attenuation, which affect measurement accuracy and fail to achieve the desired compensation effect. Kim M S calibrated the current sensors using a calibration instrument to determine the deviation between their actual output and theoretical values, and then used a time-stamped synchronization alignment algorithm to obtain the errors caused by asynchronous sampling. By combining the operational status and current characteristics of the inverter, the collected current data is analyzed in real time to identify measurement deviations caused by scaling errors and asynchronous sampling errors. Based on the constructed error compensation model, the measurement data is corrected to achieve the purpose of compensating for current measurement errors [11]. However, the accuracy of timestamps is limited by the system's clock precision. If the clock precision is low, the timestamp alignment error will be significant, making it impossible to accurately capture errors caused by asynchronous sampling, thereby affecting the accuracy of subsequent measurement error compensation.

IMU data refers to information about an object's attitude and acceleration obtained through an IMU. This data can real-time reflect the object's motion state and attitude changes [12]. Stereo vision technology, as a non-contact ranging method, simulates the principle of human binocular vision. By using two cameras to simultaneously capture an object from different angles, it obtains the object's position information [13]. This paper proposes a method for dynamic error compensation of dual-camera distance measurement for power transmission lines by integrating IMU data. The aim is to combine the real-time data provided by the inertial measurement unit to correct and compensate for the results of dual-camera visual measurements, thereby improving the accuracy and stability of power transmission line distance measurements and providing more reliable technical support for the safe monitoring and maintenance of power systems.

2. Dynamic Error Compensation for Binocular Distance Measurement of Transmission Lines

2.1. Distance Measurement of Transmission Lines Based on Binocular Vision Technology

Binocular vision technology, as a non-contact ranging method, has demonstrated great application potential in the field of power system ranging due to its high accuracy and rich information content [14]. This technology simulates the principle of human binocular vision, using two cameras to simultaneously capture an object (such as a power transmission line) from different angles. After processing by a matching algorithm, the distance between the object and the cameras is calculated based on the principle of triangulation [15].

The specific process of transmission line distance measurement based on binocular vision technology is described as follows:

2.1.1 Camera Calibration

To ensure the distance measurement accuracy of binocular vision technology, calibrating the binocular camera is a crucial step. Camera calibration refers to the process of determining the camera's internal parameters (focal length J, principal point coordinates (u_0, v_0), etc.) and external parameters (the rotation matrix R and translation vector H of the camera relative to the world coordinate system). This paper employs the camera self-calibration technique to accomplish camera calibration. This method eliminates the need for fixed calibration objects, relying instead on multiple images captured by the camera to establish image correspondences and calibrate the parameters that require determination. Among them, the expressions for the internal parameter matrix K and external parameter matrix $\left[R \middle| H\right]$ are:

$$K = \begin{bmatrix} J_x & 0 & u_0 \\ 0 & J_y & v_0 \\ 0 & 0 & 1 \end{bmatrix} \quad (1)$$

$$[R|H] = \begin{bmatrix} r_{11} & r_{12} & r_{13} & h_x \\ r_{21} & r_{22} & r_{23} & h_y \\ r_{31} & r_{32} & r_{33} & h_z \end{bmatrix} \quad (2)$$

Where J_x , J_y represent the equivalent focal length of the camera in the x and y directions. r_{ij} represents the elements in the rotation matrix, with each column representing the direction vector of a coordinate axis in the world coordinate system within the camera coordinate system, and h_x, h_y, h_z represent the translation amounts in the directions of world coordinates x, y, and z.

2.1.2 Image Acquisition

Using two calibrated cameras (left camera and right camera), mounted on a suitable platform (such as a drone, inspection vehicle, etc.), images of the power transmission line are captured from different angles at the same time to obtain left and right images. During the shooting process, it is essential to ensure that the fields of view of the two cameras have a certain overlap to facilitate matching operations.

2.1.3 Feature Point Extraction and Matching

To establish an accurate correspondence of pixel points of the power transmission line in the left and right images and eliminate spatial ambiguity caused by perspective differences, feature point extraction and matching operations are performed on the collected left and right images of the power transmission line.

Feature point extraction is achieved using the STIP algorithm, which utilizes spatiotemporal feature point detection to identify dynamic information in the images [16-17]. This paper uses the Harris3D detector as the STIP spatiotemporal feature point detector, which detects feature points in the power transmission line images by generating a second-order moment in time-space, described as:

$$\mu(\Delta\varsigma,\delta) = \hbar(\Delta\varsigma,\delta)\cdot(\nabla\varphi(\Delta,\varsigma,\delta)\cdot\nabla\varphi(\Delta,\varsigma,)^T) \quad (3)$$

Where, μ represents the time-space second-order moment, ς and δ represent the temporal and spatial scales, $\nabla\varphi$ represents the time-space gradient value, and $\hbar$ represents the smoothing function.

STIP (Spatio-Temporal Point of Interest) feature detection essentially locates key features by analyzing the spatio-temporal variations in pixel intensity in video sequences. Take the vibration monitoring of transmission lines as an example. When the lines swing in the wind, the brightness of a specific pixel area will show regular changes over time [18]. Based on the time-space second-order moment μ , the evaluation value λ used to determine STIP feature points is calculated, described as:

$$\lambda = \det(\mu) - \xi trace^3(\mu) \quad (4)$$

Where, ξ represents the adjustment coefficient.

Set the STIP spatiotemporal feature point detection threshold σ according to actual needs. When $\lambda > \sigma$, the point is determined to be a STIP spatiotemporal feature point; otherwise, it is not a feature point.

By comparing the sizes of λ and σ , effective extraction of feature points in the images of the left and right transmission lines can be achieved.

At the same time step, the matching of feature points in the images of the left and right transmission lines is divided into three steps:

First: Taking a feature point from the left transmission line image as a reference, calculate the Mahalanobis distance $\tilde{\lambda}$ to all corresponding feature points in the right image, calculated by the formula:

$$\tilde{\lambda} = \sqrt{(x_1 - x_2)^2 + (y_1 - y_2)^2} \quad (5)$$

Where, (x_1, y_1) and (x_2, y_2) represent the feature points in the images of the left and right transmission lines at the same time step.

Second: Using a brute-force matching strategy, the feature point in the right image with the smallest Mahalanobis distance to the feature point in the left transmission line image is taken as the matching point.

Third: Introduce the nearest neighbor distance ratio index to filter the matching points. For the feature points in the left image, determine the nearest matching point and the second nearest matching point, and calculate the distance ratio between the two [19]. If this ratio is less than the set threshold, the nearest matching point is determined to be the final matching point.

2.1.4 Calculation of pixel disparity

Pixel disparity is a core parameter for calculating the spatial position of objects in binocular stereo vision, defined as the difference in the x-coordinates of corresponding points (matching points) in the images of the left and right transmission lines. The disparity d is described by the formula:

$$d = x_l - x_r \quad (6)$$

Where, x_l and x_r represent the x-coordinates of the matching points in the images of the left and right transmission lines.

2.1.5 Calculate the distance from the transmission line to the camera to obtain the initial distance measurement of the transmission line

Based on the principle of triangulation and the disparity d, depth calculation can yield the distance (depth value) Z from the target point to the camera plane, which is the distance from the transmission line to the camera. This distance is taken as the initial distance measurement of the transmission line, calculated by the formula:

$$Z = (J \times B) / d \tag{7}$$

Where, J represents the focal length obtained from camera calibration, and B represents the baseline distance between the optical centers of the left and right cameras.

Based on the obtained depth value Z, the distances between the transmission lines and between the transmission line and other objects can be calculated.

2.2. Analysis of the Sources of Dynamic Errors in Binocular Distance Measurement of Transmission Lines

2.2.1 Camera motion

The camera motion is mainly manifested in two aspects: changes in camera attitude and vibrations of the camera carrying platform.

Camera attitude changes refer to changes in the pitch, yaw, and roll angles of the camera in space [20]. These changes are mainly caused by sudden camera turns, loose mechanical structures, and other factors, resulting in dynamic changes in the rotation matrix R of the camera coordinate system relative to the world coordinate system. This causes deviations in the depth information (initial distance measurements of the power transmission lines) calculated based on the initial calibration parameters, leading to dynamic errors in the distance measurement of the power transmission lines [21].

The vibrations of the camera-carrying platform are mainly observed in platforms such as drones, helicopters, and ground inspection vehicles. During the process of capturing images of the transmission line, factors such as unstable airflow, bumpy road surfaces, and vibrations from mechanical components can cause dynamic shifts in the baseline of the stereo camera (the distance between the optical centers of the two cameras), leading to a non-fixed optical center position, disrupting the geometric relationship of triangulation, and resulting in dynamic measurement errors in the distance to the transmission line.

2.2.2 The swaying of the transmission line

Power transmission conductor vibration refers to the vertical or torsional vibrations of power transmission lines caused by ice accumulation or wind excitation, resulting in dynamic changes in the spatial positions of points on the conductor surface in images [22]. During feature point matching in a binocular vision system, changes in the positions of points on the conductor surface lead to a decrease in matching accuracy. Incorrect matching results will cause errors in subsequent disparity calculations and distance estimations, thereby generating dynamic ranging errors.

2.2.3 Environmental interference

Environmental interference primarily manifests as the combined effects of temperature and humidity changes and lighting changes [23].

Temperature and humidity changes: When the temperature and humidity of the image acquisition environment undergo significant changes, the hardware parameters of the camera, optical refractive index, and physical properties of the conductor are affected. On one hand, temperature changes cause drift in camera hardware parameters—the lens shifts its focal length due to thermal expansion and contraction. On the other hand, increased humidity alters the air refractive index. The former causes the light propagation path to shift, directly resulting in ranging errors, while the latter alters the surface reflection characteristics of the conductor (enhanced diffuse reflection), making it difficult to accurately identify feature points. Additionally, temperature and humidity gradients cause uneven air density, leading to random fluctuations in light refraction paths, increasing the standard deviation of parallax estimation, and ultimately resulting in dynamic dispersion in ranging results.

Light changes: When strong direct sunlight or backlighting occurs, it causes uneven reflection on the surface of the transmission lines, leading to failed feature point extraction or mismatches. For example, under intense direct sunlight, certain areas of the conductor surface may become overexposed, making feature points unrecognizable; when shooting against the light, the conductor outline becomes blurred, making it difficult to accurately extract feature points, thereby affecting the binocular vision system's precise measurement of the distance to the transmission lines and resulting in dynamic errors.

The presence of dynamic errors leads to inaccurate binocular ranging results, causing the measured distance of the power transmission lines to deviate from the actual distance. This deviation can mislead maintenance personnel in assessing the safety status of the lines, increasing the risk of safety accidents.

2.3 IMU Data Collection

Through an analysis of the causes of dynamic measurement errors in dual-camera distance measurement of power transmission lines, it can be determined that key data include camera attitude angles (pitch, yaw, roll), platform motion states (acceleration, angular velocity), power transmission line swaying speed, and environmental information (atmospheric temperature and humidity). These parameters enable a clear understanding of the causes of dynamic errors, providing a data foundation for subsequent error compensation. The aforementioned data

can be obtained through an IMU. The IMU integrates high-precision gyroscopes, accelerometers, and other sensing devices, utilizing high-performance microprocessors and dynamic calculation algorithms to rapidly determine the real-time motion and attitude information of the target object [24-25].

To achieve consistent synchronization of motion and environmental parameters and eliminate the timing coupling effects of multi-source errors during the calculation process, this paper integrates temperature and humidity sensors into the inertial measurement unit to obtain atmospheric temperature and humidity, thereby ensuring the richness of data in the subsequent error compensation process. The IMU design block diagram is shown in Figure 1.

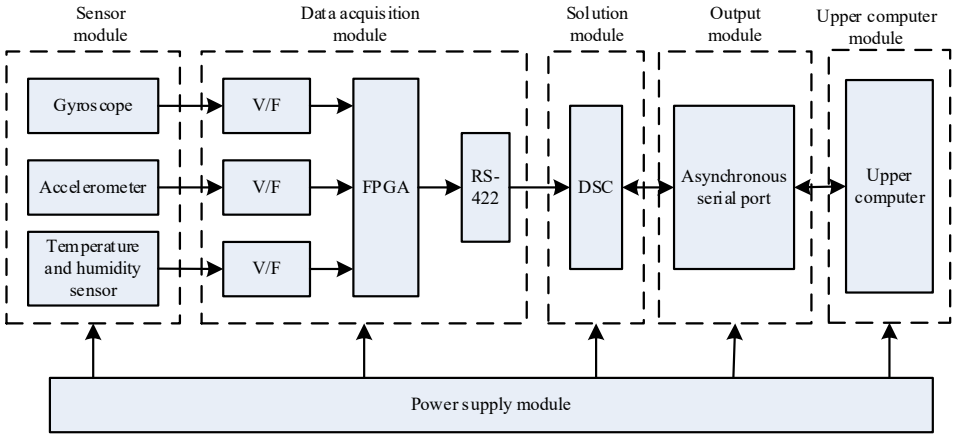

Figure 1. Block diagram of IMU design

As shown in Figure 1, the inertial measurement unit designed in this paper consists of a sensor module, a data acquisition module, a calculation module, an output module, an upper computer module, and a power supply module.

The sensor module serves as the data source for the IMU, employing gyroscopes, accelerometers, and temperature-humidity sensors to perceive real-time three-axis angles, angular velocities, carrier accelerations, transmission line accelerations, and atmospheric conditions of the stereo camera. The data acquisition module converts the analog signals output by the gyroscope, accelerometer, and temperature and humidity sensors into frequency signals with stronger anti-interference capabilities via a V/F (voltage/frequency) converter, and then transmits them to the FPGA (field-programmable gate array). The FPGA uses parallel frequency signal acquisition to perform data synchronization and preprocessing (filtering and calibration). The processed data is transmitted via an RS-422 interface to the DSP (digital signal processor) in the calculation module. In the DSP, the data is calculated and combined with navigation algorithms (such as Kalman filtering) to generate attitude angles (pitch, yaw, roll), velocity, position, and temperature and humidity parameters. Finally, the processing results are transmitted to the host computer via the asynchronous serial port (UART) of the output module, where the results are displayed. The power supply module provides stable power to the entire inertial measurement unit, ensuring the reliability of data acquisition.

The various modules of the inertial measurement unit work together to achieve IMU data acquisition.

2.4 Implementation of Dynamic Error Compensation for Stereo Distance Measurement of Transmission Lines

The dynamic error of binocular distance measurement in transmission conductors is the result of the combined effect of multiple factors. Transmission lines are in complex outdoor environments and are not only subject to changes such as dancing and thermal expansion and contraction due to natural factors like wind force, temperature and humidity, but also the camera carrying platform may experience dynamic shifts in camera posture and position during operation due to mechanical vibration and changes in its own motion state. These changes will directly or indirectly affect the accuracy of binocular ranging, causing a deviation between the measured distance and the true value. Therefore, in order to effectively enhance the accuracy of binocular distance measurement for transmission conductors, it is particularly crucial to accurately obtain the compensation amounts for various dynamic errors.

2.4.1 Acquisition of Error Compensation Amount

Although the IMU can provide high-frequency motion perception data in real time, the problem of integration drift of the IMU is particularly significant in the binocular ranging application of transmission lines. The Angle integration of the gyroscope and the velocity/position integration of the accelerometer will accumulate errors over time, causing the attitude estimation of long-term measurements to gradually deviate from the true value. The calibration requirements for sensors are strict. Temperature changes can cause zero bias and proportional factor drift, requiring frequent recalibration. IMU is sensitive to high-frequency vibration. In vibration environments such as power line inspection, noise may mask the effective signal. After analyzing the dynamic errors caused by camera motion, the swaying of transmission lines, and environmental interference, in order to improve the accuracy of stereo distance measurement of transmission lines, the collected IMU data is integrated, including camera attitude angles (pitch, yaw, roll), platform motion states (acceleration, angular velocity), transmission line swaying acceleration, and environmental information (atmospheric temperature and humidity), these limitations have been effectively overcome through multi-dimensional data fusion and closed-loop compensation mechanisms [26-27]. A multi-level error compensation system has been established, combining IMU data with visual geometric constraints. Mathematical tools such as the matrix Frobenius norm are utilized to quantify errors, avoiding reliance solely on IMU integrations. The environmental sensor provides a temperature and humidity compensation reference, which can regularly correct the zero drift of the IMU. The gallop model of the transmission line serves as an independent motion reference and forms cross-validation with the IMU data to obtain the compensation amount of various dynamic errors.

(1) Compensation for Camera Motion Errors

Changes in camera attitude are primarily manifested as dynamic shifts in the pitch, yaw, and roll angles of the three axes, leading to a time-varying rotation matrix R between the camera coordinate system and the world coordinate system. The relevant data IMU is integrated to describe this change:

$$R(t) = R_z(\gamma)R_y(\beta)R_x(\alpha) \tag{8}$$

Where, α, β, γ represent the pitch, yaw, and roll angles of the camera around the x, y, z axis, while R_x, R_y and R_z represent the rotation matrices of the corresponding axes.

If the current $R(t)$ undergoes dynamic changes while the algorithm still uses the initial calibration value $R_0(t)$, the epipolar constraint for feature point matching will become invalid, causing a shift in the disparity search range and ultimately resulting in depth errors. This yields the dynamic error compensation amount ΔZ_s due to camera pose changes, as expressed by:

$$\Delta Z_s = \frac{\tilde{Z}^2}{J} \cdot \left\| R(t) - R_0(t) \right\|_F \tag{9}$$

Where $\tilde{Z}$ represents the target depth, and $\left\| \bullet \right\|_F$ represents the Frobenius norm of the matrix.

Since the vibrations of the camera platform mainly affect the baseline of the stereo camera, error compensation is performed from both the baseline length offset and the direction offset.

First, IMU data is fused, and the linear acceleration $a(t)$ caused by the camera platform vibrations is decomposed into the baseline direction component $a_B(t)$ and the vertical component. The displacement offset $\Delta B_p(t)$ is obtained by double integrating the baseline direction acceleration, expressed by the formula:

$$\Delta B_p(t) = \iint_0 [a_B(t) - g \cdot \sin\theta(t)] dt^2 \tag{10}$$

Where, g represents gravitational acceleration, and θ represents the angle between the baseline direction and the gravitational direction (measured by the IMU pitch angle).

From this, the distance measurement error $\Delta Z_p(t)$ caused by the translational vibrations of the camera platform is derived, expressed by the formula:

$$\Delta Z_p(t) = -\frac{Z^2}{JB_0^2} \cdot B_0 \cdot \Delta B_p(t) \tag{11}$$

Where, B_0 represents the initial baseline, and Z represents the initial depth value, which is the initial distance measurement of the power transmission line.

The angular velocity $\omega(t)$ caused by the vibrations of the camera platform leads to the rotation of the stereo camera; therefore, the baseline direction offset $\Delta R_f(t)$ can be obtained by integrating the angular velocity:

$$\Delta R_f(t) = \int_0^t \omega(t) \times R_0 dt \tag{12}$$

Based on $\Delta R_f(t)$, the rotation angle $\Delta\theta_f(t)$ of the stereo camera's baseline direction is calculated, expressed by the formula:

$$\Delta\theta_f(t) = \arcsin\left(\frac{|\Delta R(t)|}{B_0} \right) \tag{13}$$

This results in the projection error during disparity calculation caused by the rotational vibrations of the camera platform, which in turn leads to distance measurement errors. The compensation amount $\Delta Z_f(t)$ for such errors is calculated using the formula:

$$\Delta Z_f(t) = Z \cdot \left(\frac{\Delta\theta_f^2(t)}{2} \right) \cdot \frac{J}{B_0} \tag{14}$$

The dynamic error compensation amounts for distance measurement caused by translational and rotational

vibrations of the camera platform are summed to obtain the dynamic error compensation amount $\Delta Z_v(t)$ caused by the vibrations of the camera platform, described as:

$$\Delta Z_v(t) = \Delta Z_p(t) + \Delta Z_f(t) \tag{15}$$

(2) Acquisition of dynamic error compensation amount for distance measurement caused by the swaying of power transmission lines

Due to the swaying of the transmission line causing instantaneous displacement of the target point in the image, combined with the swaying speed of the line, the dynamic error compensation amount ΔZ_c caused by the swaying of the transmission line is derived, and the formula is:

$$\Delta Z_c = \frac{v_c \cdot \Delta t}{\tan \vartheta} \tag{16}$$

Where, v_c represents the swaying speed of the transmission line, ϑ represents the angle between the line and the camera's optical axis, and Δt represents the image acquisition time interval.

(3) Environmental interference error compensation

The variability in the environmental temperature during image acquisition can lead to thermal expansion and contraction of the binocular camera lenses, resulting in focal length shifts. The derived dynamic error compensation amount ΔZ_w related to focal length shift is obtained, and the formula is:

$$\Delta Z_w = -\frac{Z^2}{J_0}\zeta \Delta T \tag{17}$$

Where, J_0 represents the initial focal length, ζ represents the thermal expansion coefficient of the binocular camera lens material, and ΔT represents the temperature difference.

As the environmental humidity changes, the refractive index of air will also change, causing a deviation in the light propagation path and resulting in ranging errors. The dynamic error compensation amount ΔZ_u caused by humidity changes is obtained, and the formula is:

$$\Delta Z_u = \frac{Z^2}{J_0 B_0} \cdot \frac{\Delta \rho}{\rho_0} \cdot Z \tag{18}$$

Where ρ_0 represents the initial saturated water vapor refractive index (related to humidity), and $\Delta\rho$ represents the change in refractive index.

By superimposing ΔZ_w and ΔZ_u , we obtain the dynamic error compensation amount ΔZ_h for binocular ranging of the transmission line caused by temperature and humidity changes , described as:

$$\Delta Z_h = \Delta Z_w + \Delta Z_s \tag{19}$$

Considering factors such as illumination gradient and matching errors, the dynamic error compensation amount ΔZ_g caused by changes in illumination is obtained, and the formula is:

$$\Delta Z_g = -\frac{Z^2}{f_0 B_0}\left[\frac{\Gamma_1}{G} + \Gamma_2 \cdot \sin\varphi + \kappa \cdot \frac{\nabla G}{G_0} \cdot d_0\right] \tag{20}$$

Where, Γ_1 , Γ_2 represent the illumination-matching error coefficient, φ represents the pitch angle of the binocular camera measured by the IMU (reflecting the degree of backlight/front light), κ represents the illumination sensitivity coefficient, G represents the current illumination intensity, G_0 represents the initial illumination intensity, and ∇G represents the illumination gradient.

The weighted fusion of the above dynamic error compensation quantities is carried out to obtain the total compensation amount ΔZ of the dynamic error of the transmission line binocular ranging, which is expressed as:

$$\Delta Z = w_1 \Delta Z_s + w_2 \Delta Z_v(t) + w_3 \Delta Z_c + w_4 \Delta Z_h + w_5 \Delta Z_g \tag{21}$$

Where w represents the compensation weight.

2.4.2 PID-Based Dynamic Error Compensation for Binocular Ranging of Transmission Lines

In the binocular distance measurement system for transmission conductors, due to the influence of various factors (such as environmental interference, minor deviations of the equipment itself, etc.), the measured distance will have dynamic errors. PID regulation technology can monitor and analyze these errors in real time, generate corresponding compensation instructions, and adjust the output results of the ranging system, thereby making the measurement results more accurate and stable. Applying the PID controller to dynamic error compensation in dual-camera distance measurement of power transmission lines can effectively adjust dynamic errors caused by various factors, thereby improving the measurement accuracy and stability of the dual-camera distance measurement system in dynamic scenarios [28].

The total compensation amount for the dynamic error of the binocular distance measurement of the transmission line ΔZ is input into the PID controller. Through the linear combination of the proportional, integral, and derivative components of the PID controller, the compensation amount information for the dynamic error of the binocular distance measurement is transformed into a compensation signal, generating a compensation instruction that directly acts on the distance measurement system of the transmission line. The compensated distance measurement results are then monitored in real-time by sensors, and the compensation results are fed back to the

PID controller, forming a closed-loop compensation system, thereby achieving real-time compensation for the dynamic error of the binocular distance measurement of the transmission line.

Although adaptive PID can automatically adjust parameters according to system changes, its algorithm complexity is high. In the actual complex and rapidly changing scenarios of transmission lines, it will cause response delays due to the large amount of computation. Although fuzzy logic control does not rely on precise mathematical models, the formulation of rules depends on expert experience. In scenarios with extremely high precision requirements such as binocular distance measurement for transmission lines, the completeness and accuracy of the rules are difficult to guarantee, and the computational load of the fuzzy reasoning process is also considerable. In contrast, traditional PID control can achieve efficient and stable error compensation at a lower computational cost in this study, which is more in line with the actual needs of the binocular distance measurement system for transmission conductors [29-30]. The specific steps are as follows:

(1) Generate the compensation signal for the dynamic distance measurement error

Input the total compensation amount ΔZ for the dynamic error of the binocular distance measurement of the transmission line into the PID controller to generate the compensation signal $g(t)$ for the dynamic distance measurement error, described by the formula:

$$g(t) = K_p \Delta Z(t) + K_i \int_0^t \Delta Z(t)dt + K_d \frac{d}{dt} \Delta Z(t) \quad (22)$$

Where K_p represents the proportional gain, which adjusts the output proportionally based on the current total compensation amount ΔZ , allowing for a quick response to errors and accelerating the system's response speed. K_i represents the integral gain, which accumulates past errors by integrating $\int_0^t \Delta Z(t)dt$ of the total compensation amount from time 0 to t , eliminating the system's steady-state error and making the PID output closer to the target value. K_d represents the differential gain, which is the derivative of the total compensation amount with respect to time t . It reflects the trend of ΔZ changes and can provide a compensation signal in advance when ΔZ changes rapidly, thereby reducing overshoot and improving the stability of the output results.

(2) Generate compensation instructions

Generate compensation instructions based on $g(t)$ to adjust the binocular ranging output results of the transmission line. First, normalize the error compensation signal, scaling it to the [0, 1] range to eliminate dimensional effects, and then map it to specific physical quantities (such as baseline adjustment amount, parallax offset, etc.) through a calibration formula. Then, encode the physical quantities into 16-bit/32-bit digital signals, and transmit the encoded data to the transmission line measurement system via the CAN bus to achieve the purpose of compensating for the binocular ranging errors of the transmission line.

(3) Feedback adjustment

The compensated binocular ranging results of the transmission line are fed back into the PID controller through the corresponding sensors, forming a closed-loop compensation system. That is, the PID controller calculates the difference $\varepsilon_i(t)$ between the compensated ranging result and the preset reference distance. The PID controller uses this difference to perform operational adjustments through proportional, integral, and differential components, updating and optimizing the closed-loop compensation system, continuously adjusting the compensation strategy, and gradually reducing the ranging error, thus achieving real-time compensation for the dynamic errors of the binocular ranging of the transmission line.

3. Experimental Analysis

To analyze the effectiveness of a dynamic error compensation method for dual-camera ranging of transmission lines using integrated IMU data, a 110kV/220kV overhead power line was selected as the experimental subject. The line is located in a plain terrain area, with a total length of approximately 8.6 kilometers, 19 towers, and conductors made of LGJ-240/300 type steel-core aluminum stranded wire (diameter 23.7 mm, unit length mass 0.92 kg/m, rated breaking strength 79.4 kN).

The main parameters set for this experiment are shown in Table 1.

Table 1. Main Parameters of the Experiment

Name	Selection/Value
Operating system	Ubuntu18.06
Binocular camera	Nuwa-HP60C
Gyroscope	RF-IMU406
Accelerometer	YK-YD20
Temperature and humidity sensor	JXINW-DHT11
Upper computer	TPC101-M200
Feature point extraction window radius parameter	14
Feature point detection threshold	0.06

Match the screening threshold of feature points	0.7
Frame interval	0.1s
PID sampling period	100ms
Upper limit of error	0.1

The selection of experimental parameters is based on strict engineering optimization and theoretical analysis. Among them, the setting of the PID sampling period of 100ms comprehensively considers the requirements of system real-time performance and control stability. Through frequency-domain analysis, it is determined that this value can not only effectively suppress the dynamic error corresponding to the characteristic frequency (0.1-1 Hz) of the transmission line galloping, but also avoid the controller oscillation caused by high-frequency sampling. The characteristic point detection threshold of 0.06 was determined through ROC curve analysis, which can improve the recognition rate of conductor characteristic points in complex backgrounds (such as insulators, towers and other interfering objects). The matching screening threshold of 0.7 is derived from the statistical analysis of 1000 groups of samples and can balance the contradictory demands of the false matching rate and the number of effective matching pairs. The IMU selection (RF-IMU406) can meet the accuracy requirements of wire galloping angular velocity measurement (typical value 0.5°/s) due to its zero bias stability of 0.01°/h, and its operating range of -40 to 85 ° C covers the extreme environmental demands of power inspection.

The assumptions required for this experiment are as follows:

(1) Environmental condition assumption: The research assumes that the weather conditions (such as light, wind speed, precipitation, etc.) during the experiment are within the typical inspection working conditions. The variation of light intensity between 10,000 and 100,000 Lux will not cause overexposure or underexposure of the image. The wind speed is lower than 8m/s to ensure the stability of the engineering vehicle platform. The absence of precipitation conditions ensures the cleanliness of camera lenses. This hypothetical boundary condition is satisfied by conducting experiments on sunny and windless days, but in practical applications, compensation algorithms for extreme weather need to be developed.

(2) Assumptions of the wire motion model: Wire galloping mainly presents low-frequency characteristics (0.1-1 Hz), and high-frequency vibration components can be ignored. The motion of the wires between adjacent sampling points (100 ms) can be approximately regarded as uniform acceleration motion. The galloping trajectory of the wire is smooth and continuous, with no sudden change points.

(3) Image processing assumption: The texture features of the wire surface have sufficient similarity and invariance between the left and right views; The spatial distribution of background interfering objects (such as insulators, poles and towers) has distinguishable characteristic differences from the conductors. The relative pose of the camera remains fixed after calibration.

In the experiment, a dual-camera system mounted on an engineering vehicle was employed to capture images of transmission lines, followed by feature point detection and matching. The results of feature point detection and matching are shown in Figure 2.

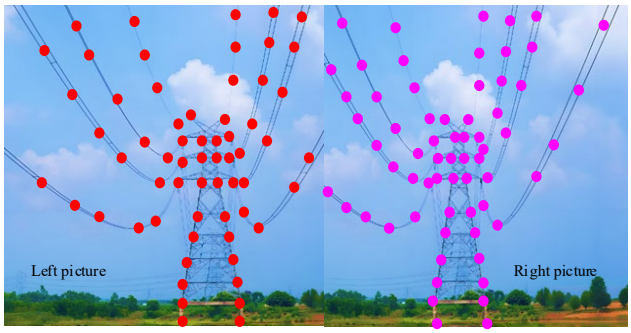

(a) Detection results of binocular image feature points of transmission lines

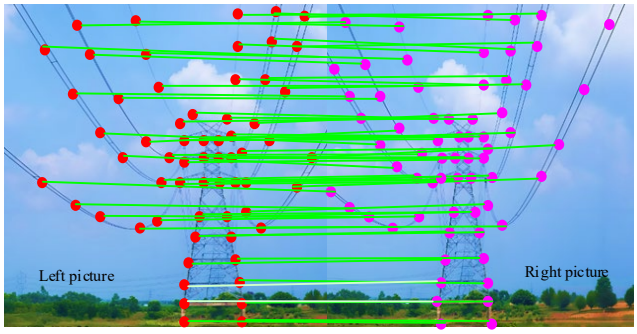

(b) Matching results of binocular image feature points of transmission lines

Figure 2. Shows the detection and matching results of binocular image feature points of transmission lines

As shown in Figure 2(a), the STIP feature point detection algorithm applied in this study can effectively filter background interference, highlight the main features of the conductor, accurately identify the key feature points in the binocular images of the transmission conductor, and precisely describe the geometric contour of the conductor and the information at the connection points with the tower. Based on the matching results in Figure 2(b), the feature point matching algorithm applied in this paper can establish a stable and reliable correspondence between the left and right binocular images based on the detected feature points. Even with a certain degree of perspective

difference, the feature points can still be matched with high accuracy, providing technical support for the distance measurement of transmission lines.

For the method proposed in this paper, the acquisition of IMU data is of critical importance, as it directly affects the accuracy of subsequent dynamic error compensation for dual-camera distance measurement of transmission lines. Therefore, this experiment adopted the peak-to-peak value of time stamp jitter (i.e., the maximum fluctuation range of time stamp errors, reflecting the synchronization risk under extreme conditions) as an indicator to quantitatively analyze the IMU data acquisition method designed in this paper from the perspective of compensation adaptability. The smaller the peak-to-peak value, the smaller the extreme timestamp offset caused by factors such as hardware trigger delay fluctuations, communication protocol jitter, or data acquisition method uncertainties during the IMU data acquisition process. This indicates that the acquired IMU data is more reliable and has a higher compatibility with the subsequent dynamic error compensation of the double-line distance measurement of power transmission lines. The results obtained from the test are shown in Figure 3.

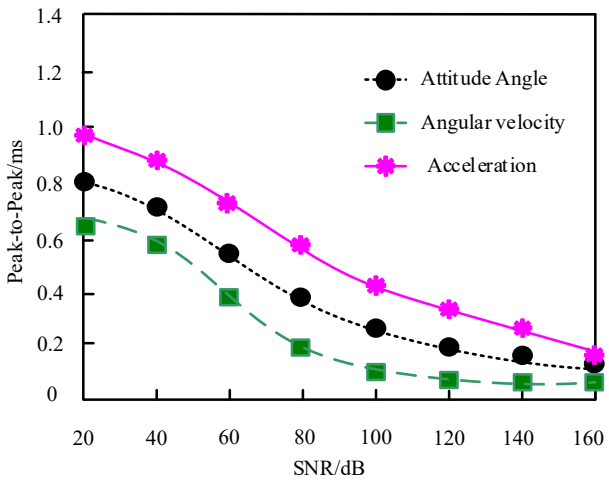

Figure 3. Shows the peak-to-peak value situation of the timestamp jitter for IMU data acquisition

As shown in Figure 3, with increasing signal-to-noise ratio (SNR), the peak-to-peak value of the timestamp jitter for IMU data (attitude angle, angular velocity, acceleration) decreases. Especially when the SNR is 160, the peak-to-peak value has dropped below 0.2 ms, and even under low SNR conditions, the peak-to-peak value remains below 1 ms. This indicates that the IMU data acquisition method proposed in this paper has synchronous robustness and is highly compatible with the subsequent dynamic error compensation of dual-camera ranging for power transmission lines.

To further analyze the performance of the method presented in this paper, the experiment evaluated the analysis using the coefficient of variation (CV) indicator. The coefficient of variation is an indicator used to measure the relative dispersion of errors, eliminating the influence of the magnitude of the error mean, and can intuitively reflect the stability of error compensation. The calculation formula for the coefficient of variation ℓ is as follows:

$$\ell=\frac{\sigma}{\eta} \tag{23}$$

Where, σ represents the standard deviation of the error after compensation, and η represents the mean of the error.

Simulate extreme weather conditions (including strong winds of force 6 (12 m/s), heavy rain (50 mm/h), and temperature shocks ranging from -20℃ to 50℃), high humidity (90%RH), and high salt fog (simulating coastal environments). The common multi-axis random vibration (0-200 Hz, acceleration 2-5 g) and shock vibration (50 g, 11 ms semi-sine wave) during the inspection of transmission lines were reproduced through the vibration table. Complex lighting variations such as strong backlight (100,000 lux), low night illuminance (0.1lux), and swaying tree shadows have been set. Typical motion patterns such as wire gallop (amplitude ±2 m, frequency 0.1-1 Hz) and sudden offset (step change 0.5 m) were simulated through a six-degree-of-freedom platform. All tests were conducted in a closed-loop control environment to ensure that each interfering factor could be precisely reproduced and quantitatively controlled, providing a reliable experimental benchmark for method validation. The range of the coefficient of variation is $[0,+\infty)$, and the closer its value is to 0, the higher the accuracy and stability of the error compensation method. The adaptive linear neuron encoder proposed in Reference [9] represents the latest progress in adaptive compensation technology based on neural networks. This method adjusts the compensation parameters through an online learning mechanism and is comparable to the PID closed-loop compensation strategy proposed in this paper in terms of adaptive characteristics. The high-speed current sensing compensation method in Reference [10] adopts advanced parallel sensing technology. The idea of multi-sensor fusion in it shares technical commonalities with the IMU-vision fusion scheme proposed in this paper. By comparing with such methods, the significant improvement of the method proposed in this paper in the key index of coefficient of variation can be better highlighted, thereby objectively proving the advancement of the proposed scheme. Therefore, the experiment tested the coefficient of variation indicator under different working conditions of power transmission lines and conducted a comparative analysis with the error compensation method based on adaptive linear neuron encoder for two-phase stepper motor vector control proposed in Reference [9] and the error analysis and compensation method for single-channel parallel current sensor current measurement in high-speed regions proposed in Reference [10], with the results shown in Figure 4.

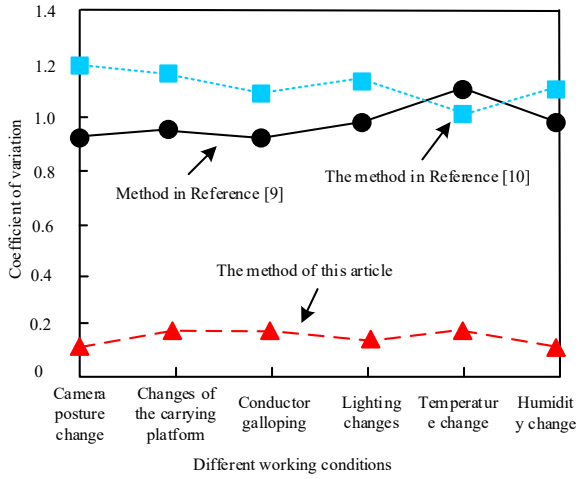

Figure 4. Coefficient of variation under different working conditions

From Figure 4, it can be seen that under different working conditions, the coefficient of variation of the method in this paper is below 0.2, significantly lower than the methods proposed in References [9] and [10]. This indicates that the method in this paper has high accuracy and anti-interference capability during the error compensation process, effectively eliminating the interference of errors on measurement results. Compared to the other two methods, it can better exert the effectiveness of error compensation under complex working conditions, providing a high-confidence accuracy guarantee for dynamic distance measurement of transmission lines.

The dynamic error convergence time reflects the speed at which the system stabilizes the error within the allowable range during the disturbance duration stage, directly affecting the availability of ranging data. The vibration of transmission lines is usually periodic. If the convergence time is too long, the system cannot complete the error correction before the next vibration period, resulting in cumulative errors. This indicator is a key parameter for measuring the dynamic tracking capability of compensation algorithms, especially crucial for monitoring the galloping of high-frequency vibrating wires. Therefore, taking the dynamic error convergence time as the index, the dynamic error convergence times of different methods are obtained as shown in Figure 5.

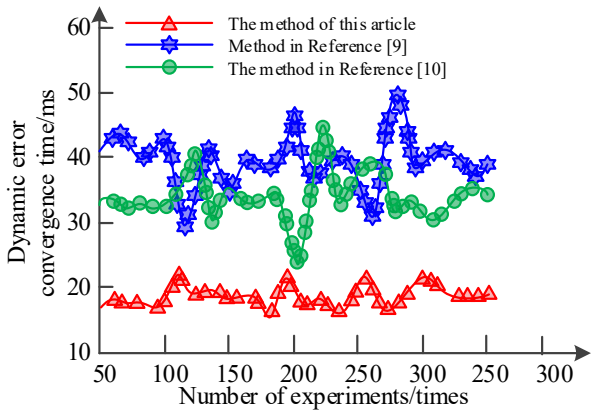

Figure 5. Dynamic error convergence times of different methods

It can be known from the experimental results in Figure 5 that the dynamic error convergence time of the method in this article is significantly lower than that of the method in Reference [10]. Its convergence time is basically stable at about 20, which is much lower than the fluctuation range of about 30-50 of the method in Reference [10]. It indicates that the method proposed in this paper can stabilize the error within the allowable range more quickly during the continuous stage of dynamic disturbance, and has better dynamic tracking ability. Especially in the high-frequency vibration scene, its advantages are significant. It can effectively avoid the cumulative error problem caused by the excessively long convergence time and improve the usability of the dynamic ranging data of transmission conductors. Compared with the method in Reference [10], it can better meet the high-precision and rapid response requirements for high-frequency vibration scenarios such as wire galloping monitoring in actual engineering.

4. Conclusion

This study proposes a dynamic error compensation method for binocular ranging of transmission conductors integrating IMU data. By fusing the high-frequency pose data of IMU with binocular vision and combining PID control, dynamic error compensation is achieved. The main innovations include: a multimodal spatio-temporal synchronization fusion architecture, a joint optimization algorithm based on error transmission, and a hybrid trigger compensation mechanism for dealing with sudden vibrations. Experiments show that this method significantly improves the ranging stability in dynamic scenes, but the current hybrid triggering mechanism is vulnerable to IMU noise and interference. In the future, the focus will be on developing LSTM vibration prediction models based on spatio-temporal attention mechanisms,

and integrating high-performance MEMS-IMU sensors to further enhance the reliability of compensation.

Acknowledgements.

This work was supported by the Science and Technology Project of State Grid Hebei Electric Power Co., Ltd. (kj2021-013).

References

[1] Parvizi P, Amidi AM, Jalilian M, Parvizi H. Useful application of machine learning methods in smart grids: a mini review. In 2024 9th international conference on technology and energy management (ICTEM), IEEE. 2024; pp. 1-7. https://doi.org/10.1109/ICTEM60690.2024.10631993

[2] Kim K, Kim I. (2023). A study on the modeling of the 154 kv power system and the prevention of reverse transmission in the incheon airport area. Transactions of the Korean Institute of Electrical Engineers. 2023; vol. 72, no. 11, pp. 1502-1506. https://doi.org/10.5370/KIEE.2023.72.11.1502

[3] Shukla PK, Deepa K. Deep learning techniques for transmission line fault classification–A comparative study. Ain Shams Engineering Journal. 2024; vol. 15, no. 2, pp. 102427-102436. https://doi.org/10.1016/j.asej.2023.102427

[4] Desta BZ, Wogari MM, Gubanski SM. Analyses of unexplained faults in transmission lines in the power grid of ethiopia. Electric Power Systems Research. 2024; vol. 231, pp. 1.1-1.12. https://doi.org/10.1016/j.epsr.2024.110293

[5] Panahi H, Abedini M, Sanaye-Pasand M. Enhancing situation awareness by determining critical intra-area and interarea transmission lines. IEEE Systems Journal. 2023; vol. 17, no. 4, pp. 6192-6201. https://doi.org/10.1109/JSYST.2023.3303339

[6] Bui NT, Nguyen TMT, Nguyen LH, Vu TTH, Nguyen CH, Bui QC, et al. Improved accuracy of optical distance sensor based on artificial neural network applied to real-time systems. Measurement Science and Technology. 2022; vol. 33, no. 7, pp. 075001-075013. https://doi.org/10.1088/1361-6501/ac527e

[7] Anand S, Kalita K, Parida SK. A novel transmission system protection scheme using optimal wide-area measurements. Electric Power Systems Research. 2023; vol. 216, pp. 1-15. https://doi.org/10.1016/j.epsr.2022.108976

[8] Kim H, Sim SH, Yoon J, Lee J. Full-scale structural displacement measurement with camera ego-motion compensation using RGB and LiDAR cameras. Measurement. 2024; vol. 237, no. 10, pp. 115194.1-115194.14. https://doi.org/10.1016/j.measurement.2024.115194

[9] Kim DH, Kim SH. Adaptive linear neuron-based encoder measurement error compensation in vector control of two-phase stepping motors. Journal of Power Electronics. 2024; vol. 24, no. 5, pp. 745-755. https://doi.org/10.1007/s43236-024-00775-8

[10] Noh YH, Lee WJ. Analysis and compensation of current measurement errors using one shunt current sensing in high-speed region. Journal of Power Electronics. 2024; vol. 24, no. 5, pp. 778-788. https://doi.org/10.1007/s43236-024-00797-2

[11] Kim MS, Park DH, Lee WJ. Compensation of current measurement errors due to sensor scale error and non-simultaneous sampling error for three-phase inverter applications. Journal of Power Electronics. 2022; vol. 22, no. 1, pp. 31-39. https://doi.org/10.1007/s43236-021-00333-6

[12] Morikawa T, Mura N, Sato TKH. Reliability and validity of estimated angles information assessed using inertial measurement unit-based motion sensors. Bio-Medical Materials and Engineering. 2024; vol. 35, no. 5, pp. 439-450. https://doi.org/10.3233/BME-240031

[13] Tohti G, Wu Z, Turhun F, Geni M, Liu S. Dynamic mode measurement method of wind turbine blade based on binocular photogrammetry. Signal, Image and Video Processing. 2025; vol. 19, no. 6, pp. 1-12. https://doi.org/10.1007/s11760-025-03989-w

[14] Stodola M, Frolík S. Self-calibration method of binocular vision based on conformal geometric algebra. Mathematical Methods in the Applied Sciences. 2024; vol. 47, no. 3, pp. 1289-1304. https://doi.org/10.1002/mma.8910

[15] Shkurti TE, Nahari A, Newman WS, Avuolu MC. (2024). Precision camera calibration using known target motions along three perpendicular axes. Optical Engineering. 2024; vol. 63, no. 2, pp. 024101.1-024101.17. https://doi.org/10.1117/1.OE.63.2.024101

[16] Krishnaveni BV, Reddy KS, Reddy PR. Indoor positioning and tracking by coupling IMU and UWB with the extended kalman filter. IETE Journal of Research. 2023; vol. 69, no. 10, pp. 6757-6766. https://doi.org/10.1080/03772063.2022.2028580

[17] Lounnas B, Benazi M, Kamel M. A robust two-step algorithm for community detection based on node similarity. Journal of Supercomputing. 2024; vol. 80, no. 16, pp. 23592-23608. https://doi.org/10.1007/s11227-024-06328-x

[18] Eristi B, Yamacli V, Eristi H. A novel microgrid islanding classification algorithm based on combining hybrid feature extraction approach with deep ResNet model. Electrical Engineering. 2024; vol. 106, no. 1, pp. 145-164. https://doi.org/10.1007/s00202-023-01977-2

[19] Kobayashi K, Sakamoto M, Soeno T, Sato T. Accuracy of an image matching technique for assessing knee alignment during the stance phase of gait using single-plane anteroposterior radiography. Bio-Medical Materials & Engineering. 2024; vol. 35, no. 6, pp. 522-529. https://doi.org/10.3233/BME-240059

[20] Paul S, Maiti TK. Accurate kinematic-parameters estimation using imu and gps sensors fusion. IEEE Sensors Journal. 2024; vol. 24, no. 21, pp. 35547-35554. https://doi.org/10.1109/JSEN.2024.3460804

[21] Moparthi JR, Bhukya KN, Chinta DP, Biswal M. Enhancing transmission line protection with adaptive ANN-based relay for high resistance fault diagnosis. Electrical Engineering. 2024; vol. 106, no. 6, pp. 7117-7132. https://doi.org/10.1007/s00202-024-02369-w

[22] Abniki H, Samsi MH, Taheri BRF. Power swing detection in parallel transmission lines connected to wind farms employing del2sg method. Journal of Electrical Engineering & Technology. 2023; vol. 18, no. 4, pp. 2567-2580. https://doi.org/10.1007/s42835-022-01348-0

[23] He H, Chen N, Gao D, Li X, Yang, M. Secure and interference-free transmission in wireless multiuser networks. IEEE Communications Letters(L-COMM). 2024; vol. 28, no. 10, pp. 2238-2242. https://doi.org/10.1109/LCOMM.2024.3450275

[24] Yu Z. A self-adaptation feature correspondences identification algorithm in terms of IMU-aided information fusion for VINS. Applied Intelligence. 2025; vol. 55, no. 3, pp. 1-12. https://doi.org/10.1007/s10489-024-06120-7

[25] Ekdahl M, Loewen A, Erdman A, Sahin S, Ulman S. Inertial measurement unit sensor-to-segment calibration comparison for sport-specific motion analysis. Sensors. 2023; vol. 23, no. 18, pp. 14-21. https://doi.org/10.3390/s23187987
[26] Lee MJ, Zhang R. Multimodal data fusion and deep learning for occupant-centric indoor environmental quality classification. Journal of Computing in Civil Engineering. 2025; vol. 39, no. 2, pp. 1.1-1.11. https://doi.org/10.1061/JCCEE5.CPENG-6249
[27] Zhang M, Sun X, Teng J, Qi L, Shen H, Li X. Standing wave compensation-based harmonic propagation mitigation for closed-loop distribution feeder. IEEE Transactions on Power Electronics. 2024; vol. 39, no. 11, pp. 14142-14147. https://doi.org/10.1109/TPEL.2024.3432311
[28] Hussain J, Zou R, Akhtar S, Abouda KA. Design of cascade P-P-FOPID controller based on marine predators algorithm for load frequency control of electric power systems. Electrical Engineering. 2025; vol. 107, no. 1, pp. 809-827. https://doi.org/10.1007/s00202-024-02551-0
[29] Hameed A, Abadi ASS, Hosseinabadi PA, Ordys A, Adouane L. Comparative analysis of a novel robust fuzzy control algorithm, MPC and PID controllers for an uncertain two-link planar manipulator robot with external disturbances. Acta Physica Polonica: A. 2024; vol. 146, no. 4, pp. 331-339. https://doi.org/10.12693/APhysPolA.146.331
[30] Halmous A, Oubbati Y, Lahdeb M. Control optimization of grid-connected pmsg wind turbine with oobo algorithm and cascade pi-pid controller. Electrical Engineering. 2024; vol. 106, no. 6, pp. 7073-7087. https://doi.org/10.1007/s00202-024-02401-z